horticulturae

MDPI

Article

A Multi-Variety Co-Expression Network Identifies Candidate Genes Associated with Tuber Color, Starch Composition and Texture in Greater Yam

Qingguang Zhou [1], Yangjing Luo [2], Erick Maledon [3], Komivi Dossa [3,4,*] and Boyun Yang [1,*]

[1] School of Life Sciences, Nanchang University, Nanchang 330031, China
[2] College of Pharmacy, Jiangxi University of Chinese Medicine, Nanchang 330004, China; 20152044@jxutcm.edu.cn
[3] CIRAD, UMR AGAP Institut, 97170 Petit-Bourg, France; erick.maledon@cirad.fr
[4] CIRAD, UMR AGAP Institut, F-34398 Montpellier, France
* Correspondence: komivi.dossa@cirad.fr (K.D.); yangboyun@163.com (B.Y.)

Abstract

Greater yam (*Dioscorea alata* L.) is a globally distributed yam species with high agronomic potential but variable culinary quality. The molecular basis of key tuber quality attributes, including flesh pigmentation, starch and sugar composition, texture after cooking, and moldability, remain poorly understood. To address this knowledge gap, we performed an integrative transcriptome analysis of six contrasting *D. alata* varieties representing diverse tuber quality profiles. RNA-seq data were integrated with biochemical, morphological, textural, and flesh-color phenotypes to identify genes associated with quality variation. Differential expression and pathway enrichment analyses revealed major changes in phenylpropanoid, flavonoid, carotenoid, galactose, zeatin, and photosynthesis-related pathways. Weighted gene co-expression network analysis identified 26 expression modules, five of which were associated with specific varieties and quality traits. Candidate genes were prioritized by integrating co-expression modules, differential expression patterns, and functional annotation. Anthocyanin- and flavonoid-related genes and regulators (including *CCoAOMT*, *C3H*, *F3′H*, *F3′5′H*, *DFR*, *AP2*, *MYB*, *WD40*) were associated with purple flesh, whereas carotenoid biosynthetic genes (*PSY* and *NCED*) were linked to yellow flesh. Modules associated with starch, sugar and moldability highlighted genes involved in carbohydrate metabolism and cell wall modification, including beta-glucosidase, glycosyl hydrolases, pectinesterase, and galacturonidase. By simultaneously analyzing six genetically diverse varieties, this study extends previous pairwise transcriptomic comparisons and provides a comprehensive candidate-gene resource for improving tuber quality in *D. alata*.

Keywords: root and tuber crop; tuber quality; WGCNA; anthocyanin; carotenoid; starch

Check for updates

Academic Editor: Shi Liu

Received: 2 August 2026
Revised: 27 September 2026
Accepted: 28 September 2026
Published: 2 October 2026

Copyright: © 2026 by the authors. Licensee MDPI, Basel, Switzerland. This article is an open access article distributed under the terms and conditions of the Creative Commons Attribution (CC BY) license.

1. Introduction

Yams (*Dioscorea* spp.) are major tropical tuber crops that support food security, income generation and cultural practices across Africa, Asia, the Pacific and the Caribbean [1–3]. Among cultivated yams, *D. alata*, also known as greater yam or water yam, is one of the most widely distributed species. It combines high yield potential, broad adaptation and tolerance to several production stresses, making it an attractive species for breeding and deployment in diverse production systems [3,4].

Despite these advantages, the adoption and market value of *D. alata* varieties are strongly shaped by tuber quality. Consumers and processors evaluate yam according to visible flesh color, dry matter, starch content, sugar content, cooking behavior, hardness and the capacity of boiled tissue to form a cohesive pounded product [5,6]. These traits are complex, partially correlated and difficult to measure across large breeding populations. Near-infrared spectroscopy, quantitative trait loci mapping and association mapping strategies have recently improved phenotyping and genetic dissection of *D. alata* quality traits, including dry matter, oxidative browning, cooking time, hardness and moldability [7–13].

Molecular studies of yam tuber quality have largely focused on single contrasts or specific pathways. RNA-seq analysis of purple and white *D. alata* tubers identified flavonoid biosynthesis genes associated with purple pigmentation [14]. More recent integrated transcriptome and metabolome studies confirmed the central role of flavonoid and anthocyanin metabolism in *D. alata* tuber color, including differential accumulation of flavonoids and cyanidin-derived anthocyanins in purple tissues [15,16]. Anthocyanin profiling in Thai purple *D. alata* tubers has also documented anthocyanin accumulation in purple yam flesh [17]. These results are consistent with the broader roles of flavonoids, anthocyanins and carotenoids in plant tissue pigmentation [18–21]. In parallel, transcriptome and metabolome analyses of yam tuber development in *D. polystachya* highlighted starch and sucrose metabolism, hormone signaling and flavonoid pathways as major components of tuber growth and storage-organ quality [22]. However, the transcriptional regulation of multiple tuber quality traits has not been investigated across contrasting *D. alata* varieties. A panel that contrasts flesh color, carbohydrate composition and textural traits can reveal whether common or partially distinct co-expression patterns are associated with these quality dimensions. Co-expression networks are useful for this question because they detect coordinated gene modules and relate them to biological traits [23,24]. Weighted gene co-expression network analysis (WGCNA) provides a statistical framework for defining such modules and linking module eigengenes to phenotypes [25]. WGCNA has been successfully applied to decipher diverse agronomic and quality traits. In apple, co-expression network analyses identified modules associated with anthocyanin accumulation and uncovered key *MYB* regulators controlling fruit coloration beyond those detected by conventional differential expression analysis [26]. Similarly, transcriptome-wide network analyses during apple fruit development identified modules associated with sugar accumulation and organic acid metabolism, providing insights into the coordinated regulation of fruit quality [27]. WGCNA has also been widely used to characterize regulatory networks associated with secondary metabolism, developmental processes and responses to environmental stresses in diverse crop species, highlighting its utility for prioritizing biologically meaningful candidate genes within complex quantitative traits [28,29].

Here, we analyzed tuber RNA-seq data from six *D. alata* varieties selected for contrasting tuber quality traits. We combined differential expression, functional enrichment and WGCNA to identify candidate genes and modules associated with visible flesh pigmentation, biochemical composition (starch and soluble sugar contents), tuber morphology and cooking-related texture. The main methodological innovation of this work is the integration of a multi-variety tuber quality panel with co-expression networks, allowing candidate-gene prioritization.

2. Materials and Methods

2.1. Plant Material and Tuber Sampling

Six *Dioscorea alata* varieties contrasting for mature tuber quality traits (CIRAD121, CIRAD174, CIRAD136, CIRAD154, CIRAD137, and CIRAD165) were selected from the CIRAD germplasm collection in Guadeloupe. Ten seed-tuber fragments per variety were

planted in May 2020 at the Roujol research station, CIRAD, Guadeloupe (16°11′26″ N, 61°35′27″ W). All six varieties were grown in a single ridge under identical field conditions. Plants of the same variety were spaced 30 cm apart within the ridge, while adjacent varieties were separated by 5 m to facilitate field management and minimize interference among accessions. No staking was applied and the crop was managed without mineral fertilizers, herbicides, or chemical treatments. Weed growth was controlled by covering the ridges with cardboard mulch before plantation. Mature tubers were harvested manually in February 2021. For each variety, tubers from three independent plants were randomly selected as biological replicates for RNA sequencing. Tuber flesh was washed, peeled, immediately frozen in liquid nitrogen, and stored at −80 °C until RNA extraction.

2.2. Phenotypic Traits Used for Transcriptome Interpretation

The phenotypic dataset used for transcriptome interpretation was derived from previous studies on the same six varieties and was therefore independent of the biological tubers used for RNA sequencing in the present study. The six varieties had previously been characterized for biochemical, textural and external tuber quality traits based on protocols described by Ehounou et al. [10], Dossa et al. [12] and Houngbo et al. [30]. The dataset included flesh color, dry matter, protein, total starch, total soluble sugars, amylose content, starch-granule projected area, texture-related traits (hardness, cohesiveness, springiness and moldability), and tuber morphological descriptors.

Flesh color was assessed by direct visual inspection and classified as white, yellow-cream, or purple. Dry matter (% fresh weight), protein (% dry weight), total starch (% dry weight), total soluble sugars (% dry weight), amylose (% total starch), starch-granule projected area (μm^2), hardness (N), cohesiveness, springiness and moldability were determined as previously described [9,12,13,30]. Moldability was assessed using an ordinal score ranging from 1 to 3, where 1 = not moldable, 2 = acceptable moldability, and 3 = highly moldable. Results are presented as mean ± standard deviation of three biological replicates. The quantitative phenotypic data were subjected to analysis of variance and post hoc means separation were conducted by Duncan Multiple Range Test at $p < 0.05$ using Minitab 22.4 software (Minitab LLC, State College, PA, USA). Morphological traits were scored according to the yam descriptor scale described by Ehounou et al. [10]. Tuber length-to-width ratio (L/W) was calculated by dividing tuber length by its maximum width. Tubercular roots were scored as 1 = few tubercular roots, and 2 = abundant tubercular roots. Skin texture was scored as 1 = smooth and 2 = rough. Shape regularity was scored as 1 = regular, 2 = irregular, and 3 = highly irregular.

2.3. RNA Extraction, Library Preparation and Sequencing

Total RNA was extracted from mature tuber tissue using the Spectrum Plant Total RNA kit (Sigma-Aldrich, St. Louis, MO, USA) with DNase treatment. RNA concentration was measured with Quant-iT RiboGreen RNA reagent (Invitrogen™, Thermo Fisher Scientific, Eugene, OR, USA), and RNA quality was assessed using an Agilent 5200 Fragment Analyzer (Agilent Technologies, Santa Clara, CA, USA). Eighteen RNA-seq libraries (6 varieties × 3 biological replicates) were prepared from 1 µg of total RNA using the TruSeq RNA Sample Preparation v2 kit (Illumina Inc., San Diego, CA, USA) and sequenced as 150 bp paired-end reads on an Illumina HiSeq 3000 platform (Illumina Inc., San Diego, CA, USA).

2.4. Read Processing and Transcript Quantification

Raw read quality was assessed with FastQC v0.11.7 [31]. Adapter sequences and low-quality bases were removed with Trimmomatic v0.39 [32]. Trimmed reads were quantified against the *D. alata* V2_1 (https://phytozome-next.jgi.doe.gov/info/Dalata_v2_1,

accessed on 12 January 2026) genome assembly [3] using Kallisto v0.46.1 [33], which generated transcript abundance estimates as both estimated counts and transcripts per million (TPM). TPM values were used for exploratory expression analyses and visualization, where abundance values from biological replicates were averaged by variety and transformed as $\log_{10}(\text{TPM} + 1)$ or $\log_2(\text{TPM} + 1)$, depending on the analysis.

2.5. Differential Expression and Pathway Enrichment

Differential expression analysis was performed using gene-level estimated counts obtained from Kallisto v0.46.1 transcript quantifications and imported with *tximport* prior to statistical analysis. Genes with total counts < 10 across all samples were removed before analysis. Differential expression was evaluated across all 15 pairwise comparisons among the six varieties using a negative-binomial framework implemented in DESeq2 v3.23 [34,35]. For each pairwise comparison, genes with $|\log_2 FC| > 1$ and a Benjamini–Hochberg false discovery rate (FDR) < 0.05 [36] were retained. The resulting gene lists from all 15 pairwise comparisons were then merged into a non-redundant set of differentially expressed genes, which was used for downstream Kyoto Encyclopedia of Genes and Genomes (KEGG) pathway enrichment analysis. KEGG pathway enrichment analysis was performed using KOBAS [37,38]. The significantly differentially expressed genes were tested against the complete set of annotated genes in the *D. alata* V2_1 genome [3], which served as the background gene universe. *p*-values were adjusted for multiple testing using the Benjamini–Hochberg FDR, and pathways with FDR < 0.05 were considered significantly enriched.

2.6. Weighted Gene Co-Expression Network Analysis

The expressed genes were used to construct a weighted co-expression network with the WGCNA R package [25]. Raw count data were normalized using the variance stabilizing transformation implemented in DESeq2 v3.23 prior to WGCNA. The resulting variance-stabilized expression values were used for network construction with following parameters: the network type (unsigned), correlation method (Pearson correlation), minimum module size (100 genes), module-merging threshold (mergeCutHeight = 0.25), and the scale-free topology parameters (soft-thresholding power $\beta = 7$, corresponding to a signed $R^2 = 0.90$). Module eigengenes were correlated with varieties and tuber quality traits, following the principle that coordinated transcript modules can reveal biological programs more robustly than isolated genes [23,24]. Continuous traits were analyzed using their measured quantitative values. Binary categorical traits (e.g., skin texture and tubercular roots) were encoded as 0/1 variables. Nominal variables with more than two categories, including variety identity and flesh-color class, were transformed into binary indicator (dummy) variables, with one binary vector generated for each category (e.g., CIRAD121 = 1 for samples from CIRAD121 and 0 otherwise). Moldability was evaluated on an ordinal three-level scale (1–3) and was analyzed as a numeric variable because the ordered categories represent an increasing phenotypic gradient, consistent with common practice for exploratory WGCNA module–trait correlation analyses. Module eigengenes were then correlated with these binary trait vectors using Pearson correlation, following the standard WGCNA framework. Modules with absolute module–trait correlation at least 0.60 and an adjusted *p* (FDR) < 0.05 were considered strongly associated with the corresponding traits and were prioritized for candidate-gene identification. Because phenotypic measurements were obtained from previous studies and not from the RNA-seq tubers, the mean phenotypic value of each variety was assigned to its three biological RNA-seq replicates for the module–trait correlation analysis. Accordingly, module–trait correlations should be interpreted as associations between gene co-expression patterns and stable differences among varieties. To evaluate whether module summaries were

disproportionately influenced by any single sample, we performed a leave-one-sample-out jackknife stability analysis. In each of 18 iterations, one sample was omitted and each module eigengene was recalculated as the first principal component of standardized expression profiles. Stability was quantified as (i) the Pearson correlation between the jackknife and full-data eigengene scores across the retained samples and (ii) the Spearman correlation between the corresponding gene module-membership rankings.

2.7. qRT-PCR Validation Panel

To validate the RNA-seq results, fifteen candidate genes were selected following an integrative prioritization strategy. Candidate genes were required to (i) be significantly differentially expressed, (ii) belong to WGCNA modules significantly associated with the corresponding tuber quality traits and varieties ($|r| \geq 0.60$, $p < 0.05$), and (iii) have functional annotations consistent with the biological pathways associated with the investigated traits. Representative genes from the major pathways identified in this study were subsequently selected for qRT-PCR validation. The same RNA samples used for transcriptome sequencing were reverse-transcribed into first-strand cDNA. For each sample, 1 μg of total RNA was used for cDNA synthesis with SuperScript III Reverse Transcriptase (Invitrogen, Carlsbad, CA, USA). Gene-specific primers were designed with Primer 5.0 (Supplementary Table S1). Quantitative real-time PCR was performed on an Applied Biosystems 7500 Real-Time PCR System (Applied Biosystems, Foster City, CA, USA) using three biological replicates and three technical replicates per sample. Amplifications were carried out in 20 μL reaction volumes containing SYBR Green PCR Master Mix (Takara, Dalian, China). The thermal cycling program consisted of an initial denaturation at 95 °C for 5 min, followed by 35 cycles of 95 °C for 30 s, 60 °C for 30 s, and 72 °C for 30 s. Expression levels were normalized against the *D. alata ACTIN18* reference gene, and relative transcript abundance was calculated using the $2^{-\Delta\Delta Ct}$ method [39]. Because qRT-PCR validation was performed separately for several pairwise contrasts, no single calibrator was used across all analyses. Instead, for each contrast, one genotype was designated as the calibrator, and the relative expression of the contrasting genotype was calculated accordingly. Differences in gene expression among varieties were evaluated by one-way analysis of variance followed by Tukey's honestly significant difference test at $p < 0.05$ using Minitab 22.4 software (Minitab LLC, State College, PA, USA). To validate the RNA-seq expression profiles, Pearson's correlation analysis was performed between RNA-seq and qRT-PCR expression estimates for the selected candidate genes. RNA-seq expression values corresponded to normalized $\log_2$ fold changes, while qRT-PCR relative expression values ($2^{-\Delta\Delta Ct}$) [39] were $\log_2$-transformed prior to analysis to ensure comparable data scales.

2.8. Manuscript Drafting and Language Editing

DeepL Write (DeepL SE, Cologne, Germany) was used solely to improve the English language, grammar, and readability of the manuscript. All suggestions were carefully reviewed, accepted or rejected by the authors as appropriate, and the authors take full responsibility for the final content of the manuscript.

3. Results

3.1. The Six Varieties Capture Visual, Biochemical and Textural Variation in Mature Tuber Quality

The six *Dioscorea alata* varieties exhibited substantial variation in tuber morphology, flesh color, biochemical composition and textural properties (Table 1; Figure 1). Flesh color ranged from white to purple, with CIRAD136 displaying a purple flesh, CIRAD121, CIRAD165 and CIRAD154 exhibiting yellow-cream flesh, and CIRAD137 and CIRAD174 showing white flesh. Marked differences were also observed in tuber biochemical com-

position. Protein content ranged from 4.22% in CIRAD174 to 6.47% in CIRAD154, while starch content varied from 74.09% (CIRAD154) to 83.08% (CIRAD137). Soluble sugar concentration showed even greater variation, with CIRAD154 accumulating the highest level (6.74%), approximately six-fold higher than CIRAD174 (1.05%). Dry matter content ranged from 22.29% in CIRAD154 to 31.40% in CIRAD137, whereas amylose concentration varied between 22.99–23.11% in CIRAD154 and CIRAD136 and approximately 30% in CIRAD174. The six varieties also differed in starch granule morphology and cooking-related texture. Mean starch granule area ranged from 689.5 μm^2 in CIRAD154 to 1166.6 μm^2 in CIRAD137. Instrumental texture analysis revealed considerable differences in hardness, cohesiveness, springiness and moldability. Hardness varied nearly fourfold, from only 2.22 N in CIRAD154 to 8.50 N in CIRAD137. Cohesiveness and springiness were highest in CIRAD165 and CIRAD154, whereas moldability, an important quality attribute for the preparation of pounded yam, reached its highest values in CIRAD174 and CIRAD137 and remained comparatively low in the other four varieties.

Table 1. Phenotypic variation among the six *D. alata* varieties used for RNA-seq analysis.

Traits	Varieties					
	CIRAD121	**CIRAD174**	**CIRAD136**	**CIRAD137**	**CIRAD154**	**CIRAD165**
Flesh color	Yellow-cream	White	Purple	White	Yellow-cream	Yellow-cream
Protein (%)	4.50 ± 0.82 b	4.22 ± 1.10 b	5.73 ± 0.41 a	5.38 ± 0.06 ab	6.47 ± 1.15 a	5.62 ± 1.15 ab
Total starch (%)	75.54 ± 3.62 b	80.92 ± 1.76 a	79.44 ± 0.28 a	83.08 ± 3.92 a	74.09 ± 5.07 b	81.89 ± 2.73 a
Total soluble sugars (%)	3.39 ± 0.17 b	1.05 ± 0.18 c	3.10 ± 0.12 bc	2.41 ± 0.81 bc	6.74 ± 3.52 a	2.65 ± 0.57 bc
Starch grain projected area (μm^2)	921.30 ± 121.30 a	974.10 ± 174.08 a	1008.60 ± 308.64 a	1166.60 ± 166.58 a	689.50 ± 69.47 b	1057.40 ± 143.41 a
Dry matter (%)	29.93 ± 1.26 b	29.81 ± 1.14 b	29.86 ± 1.19 b	31.40 ± 2.73 a	22.29 ± 6.38 c	28.72 ± 0.05 b
Amylose (%)	29.31 ± 1.97 a	30.39 ± 3.04 a	23.11 ± 4.23 b	28.91 ± 1.57 a	22.99 ± 4.35 b	29.34 ± 2.00 a
Hardness (N)	5.11 ± 0.49 d	7.50 ± 1.91 b	6.08 ± 0.49 c	8.50 ± 2.91 a	2.22 ± 0.37 f	4.14 ± 1.46 e
Cohesiveness	0.16 ± 0.02 b	0.25 ± 0.06 ab	0.20 ± 0.12 ab	0.28 ± 0.03 ab	0.47 ± 0.16 ab	0.53 ± 0.21 a
Springiness	0.13 ± 0.09 c	0.34 ± 0.03 ab	0.20 ± 0.18 b	0.34 ± 0.03 ab	0.65 ± 0.28 a	0.59 ± 0.21 a
Moldability *	1.01 ± 0.36 b	2.01 ± 0.65 a	1.05 ± 0.32 b	1.82 ± 0.45 a	1.02 ± 0.34 b	1.29 ± 0.08 b
Tubercular roots *	2	2	2	1	1	1
Shape regularity *	2	1	2	2	2	1
Ratio length/width	9.56 ± 5.66 a	3.45 ± 0.46 c	3.23 ± 0.68 d	1.50 ± 0.41 f	1.80 ± 0.11 e	3.91 ± 0.60 b
Skin texture *	2	1	1	1	2	1

Mean ± standard deviation in a row with a common alphabet indicates no significant difference by Duncan multiple range test at the 5% probability level. * Explanations of the values for these traits can be found in the Methods Section.

Substantial variation was likewise observed for tuber morphology. The ratio of tuber length to width ranged from 1.50 in CIRAD137, indicative of rounded tubers, to 9.56 in CIRAD121, which produced highly elongated tubers. Skin texture, shape regularity and the abundance of tubercular roots also varied. Overall, these six varieties represent a broad spectrum of phenotypic diversity encompassing pigmentation, biochemical composition, starch characteristics, cooking quality and tuber morphology, thereby providing a suitable panel for investigating the molecular basis associated with variation in yam tuber quality traits.

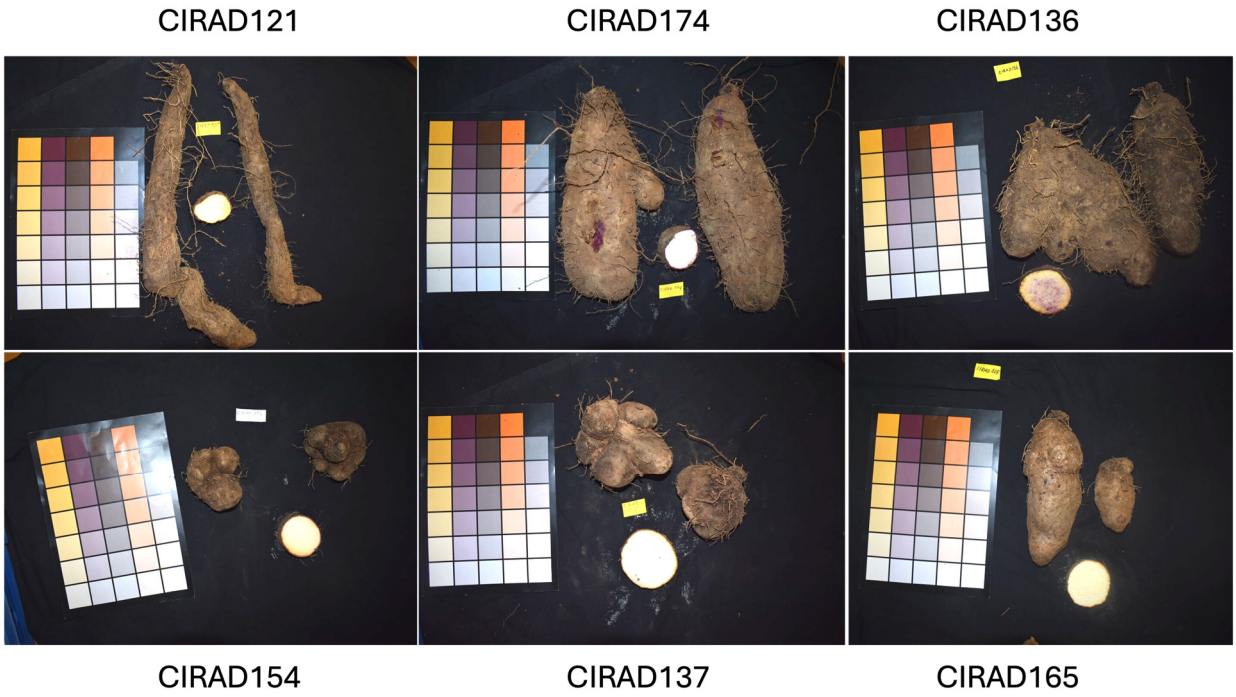


Figure 1. Phenotypic diversity of the six *D. alata* varieties used for tuber RNA-seq. The figure shows visual flesh-color classes and external tuber morphology.

3.2. RNA-Seq Profiles Separate Varieties According to Mature Tuber Expression

Across the 18 RNA-seq libraries, 15.55–33.81 million raw paired-end fragments were generated per sample. After adapter and quality trimming, 94.00–97.15% of the fragments were retained. Alignment rates ranged from 72.49 to 81.01%. The reference expression matrix comprised 25,188 gene models, of which 18,633–20,521 showed detectable expression (TPM > 0) in individual libraries (Supplementary Table S2). Principal component analysis based on transcript abundance separated the varieties, with the first two principal components explaining 57.4% and 28.6% of the total expression variation, respectively, for a cumulative 86% of the variance (Figure 2). The three biological replicates clustered according to variety, with only limited within-variety dispersion expected from independent tubers collected from different plants. This pattern indicates that biological variation among varieties exceeded within-variety variation, supporting the reproducibility of the sampling strategy and the overall reliability of the RNA-seq dataset.

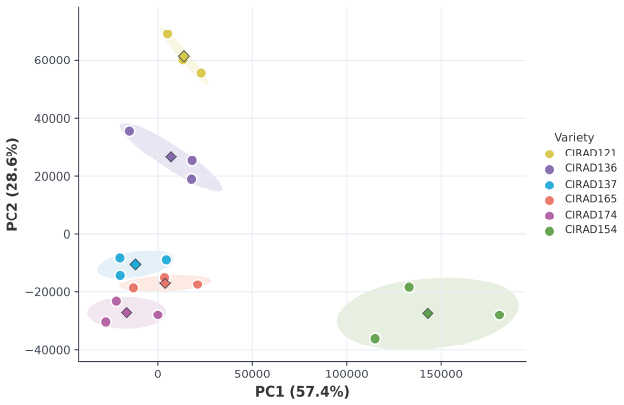


Figure 2. Transcriptome-wide expression structure among six *D. alata* varieties. Principal component analysis was performed using transcript abundance values from 18 libraries. The first two axes explained 57.4% and 28.6% of expression variation, respectively.

3.3. Pairwise Contrasts Reveal Large Expression Difference Among Varieties

Across the 15 pairwise comparisons among the six varieties, the number of genes showing $|\log_2FC| > 1$ ranged from 4812 in the CIRAD174 versus CIRAD137 comparison to 8206 in the CIRAD165 versus CIRAD136 comparison (Figure 3; Supplementary Table S3). After applying a Benjamini–Hochberg adjusted FDR < 0.05 within each comparison and merging the resulting significant gene lists, we obtained a non-redundant set of 9476 unique differentially expressed genes (DEGs). These DEGs were subsequently used for KEGG pathway enrichment analysis. Twenty-four pathways were significantly enriched, including phenylpropanoid biosynthesis, flavonoid biosynthesis, galactose metabolism, zeatin biosynthesis and photosynthesis-related pathways (Supplementary Table S4). These enrichments indicate that mature tuber quality differences involve pigmentation, carbohydrate-associated metabolism and regulatory processes.

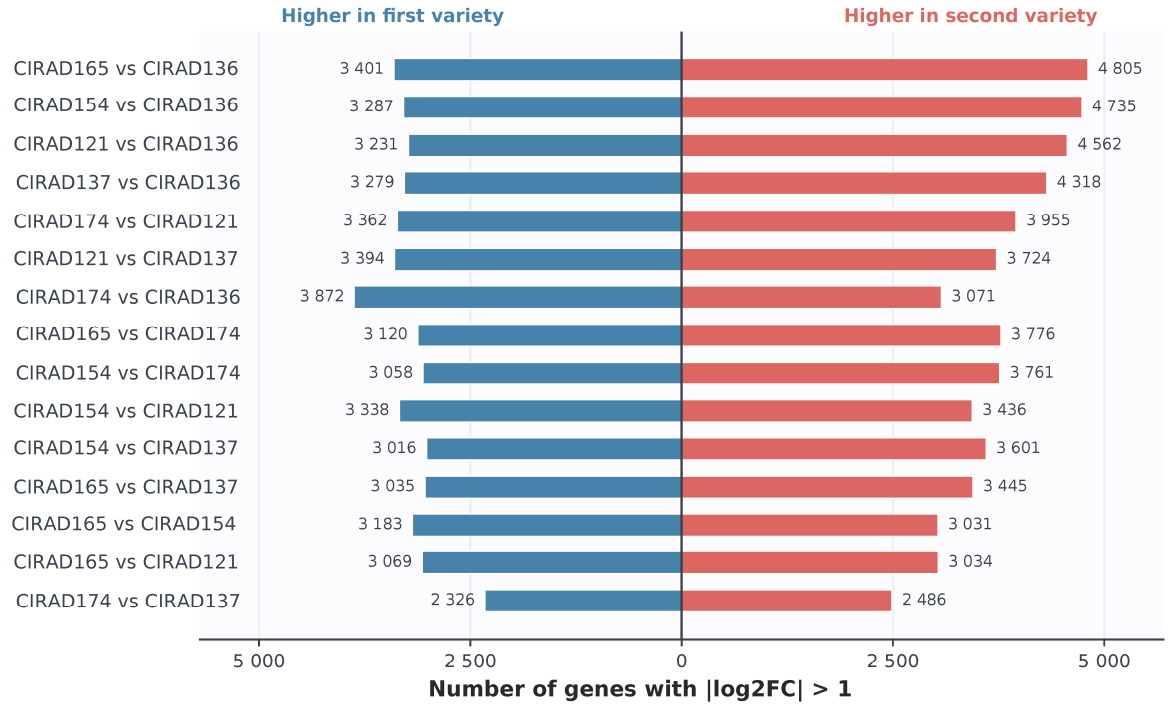


Figure 3. Expression landscape across 15 pairwise comparisons among the six *D. alata* varieties. Horizontal bars summarize the number of genes with $|\log_2FC| > 1$ per contrast; left-facing bars represent genes expressed at higher levels in the first variety of each comparison, whereas right-facing bars represent genes expressed at higher levels in the second variety.

3.4. Co-Expression Analysis Resolves Trait-Associated Modules

Weighted gene co-expression network analysis of the complete normalized expression dataset identified 26 co-expression modules, providing a network-level view of tuber quality variation beyond individual differential expression analyses (Figure 4A, Supplementary Figure S1). Module–trait correlation analysis identified co-expression patterns associated with combinations of variety identity and tuber quality traits. Several modules were significantly associated either with individual varieties or with specific quality traits alone. To maximize biological relevance, we focused on modules showing concurrent associations with both a variety and one or more phenotypic traits (Benjamini–Hochberg adjusted FDR < 0.05), reasoning that such modules were more likely to represent transcriptional programs associated with the observed phenotypic variation. Based on this criterion, five modules ("blue", "red", "purple", "cyan" and "orange") were selected for downstream analyses because they exhibited strong and significant associations with at least one variety and

one quality-related trait (Figure 4B,C; Table 2). Module color names are arbitrary WGCNA labels and do not correspond to tuber flesh-color categories.

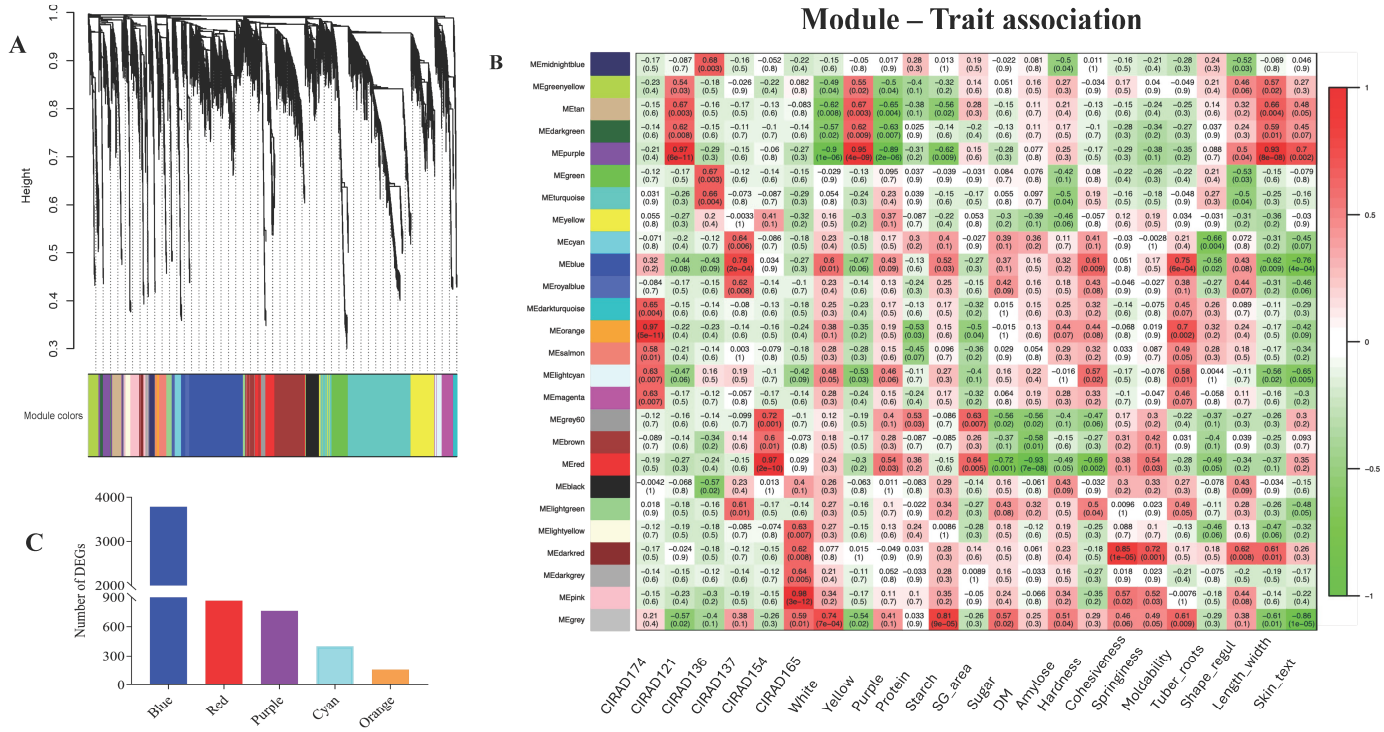


Figure 4. Co-expression network analysis links gene modules to tuber quality traits. (**A**) Clustering dendrograms of selected genes. Different colors represent different gene modules, and twenty-six modules were identified. (**B**) Module–varieties–trait relationships. Each row corresponds to a module eigengene. (**C**) Bar plot of number of differentially expressed genes detected on the selected modules. Module color names are arbitrary WGCNA labels and do not correspond to tuber flesh-color categories.

Table 2. Trait-associated WGCNA modules retained for candidate-gene mining.

Module *	Blue	Red	Purple	Cyan	Orange
Variety	CIRAD137 (0.78)	CIRAD154 (0.97)	CIRAD121 (0.97)	CIRAD137 (0.64)	CIRAD174 (0.97)
Trait	Moldability (0.75)	SG_area (−0.72)	Flesh color class (−0.9; 0.95; −0.89)	Tubercular roots (−0.66)	Moldability (0.70)
Trait	L/W (−0.62)	Hardness (−0.69)	Starch (−0.62)	-	-
Trait	Skin texture (−0.76)	Sugar (0.64)	L/W (0.93)	-	-
Trait	-	-	Skin texture (0.70)	-	-

Values in parentheses represent Pearson correlation coefficients with Benjamini–Hochberg adjusted FDR < 0.05. L/W = ratio of length to width; SG_area = starch grain projected area. Flesh pigmentation refers to visual tuber flesh categories. * Module color names are arbitrary WGCNA labels and do not correspond to tuber flesh-color categories.

Candidate genes were subsequently prioritized within these modules by integrating three complementary criteria: high module membership, functional annotation in biologically relevant pathways, and significant differential expression between phenotypically contrasted varieties. Accordingly, anthocyanin-related candidates were identified from the CIRAD136 versus CIRAD137 comparison, carotenoid-associated genes from the CIRAD121 versus CIRAD174 comparison, and genes potentially involved in moldability from contrasts involving CIRAD174 and CIRAD121.

The "purple" module exhibited the strongest association with CIRAD121, a yellow-fleshed variety characterized by low starch content and elongated tubers. Consistent with

this phenotype, the module was simultaneously correlated with flesh color (positively with yellow but negatively with purple and white flesh colors), starch content, tuber length-to-width ratio and skin texture, suggesting coordinated regulation of yellow pigmentation, carbohydrate metabolism and tuber development. The remaining selected modules defined additional co-expression patterns associated with specific varieties and their characteristic quality profiles. The "orange" module was specifically associated with CIRAD174 and high moldability, the "cyan" module with CIRAD137 and tubercular-root development, the "red" module with CIRAD154, high sugar content and low starch-grain area, whereas the "blue" module was associated with CIRAD137 together with high moldability, tuber shape and skin texture.

The jackknife (leave-one-sample-out) analysis indicated that the five modules prioritized for candidate-gene mining were not driven by any single sample. Their minimum eigengene agreement across sample omissions ranged from r = 0.989 for the "cyan" module to r > 0.999 for the "blue", "red", "purple" and "orange" modules. Minimum agreement of gene module-membership rankings ranged from Spearman rho = 0.992 to 1.000 (Supplementary Table S5). These findings support the within-dataset stability of the selected modules.

Collectively, these results indicate that tuber quality variation is associated with multiple co-expression modules, each linked to specific combinations of genotype and phenotype. By prioritizing modules jointly supported by genotype and phenotype associations, our framework increases confidence that the selected co-expression networks capture biologically meaningful mechanisms associated with yam tuber quality. This strategy provided a robust basis for prioritizing candidate genes potentially contributing to the major quality attributes investigated in this study.

3.5. Pigmentation Module Prioritizes Anthocyanin, Carotenoid and Transcription-Factor Candidates

Within the "purple" module, pathway annotation highlighted genes from phenylpropanoid, flavonoid and carotenoid metabolism. Six structural candidates from the phenylpropanoid/flavonoid branch were more highly expressed in the purple-fleshed variety CIRAD136 than in the white-fleshed variety CIRAD137: *Dioal.02G073700.1* (caffeoyl-CoA O-methyltransferase), *Dioal.19G068100.1* (coumaroylquinate (coumaroyl shikimate) 3′-monooxygenase), *Dioal.03G018800.1* (flavonoid 3′-monooxygenase), *Dioal.07G104800.1* (flavonoid 3′,5′-hydroxylase), and two bifunctional dihydroflavonol 4-reductase/flavanone 4-reductase genes, *Dioal.04G075100.1* and *Dioal.20G036200.1* (Figure 5). These genes occupy key steps in phenylpropanoid-to-anthocyanin metabolism and overlap with flavonoid pathway genes reported in earlier purple-versus-white *D. alata* transcriptome studies [14–16]. The coordinated up-regulation of multiple structural genes spanning successive steps of the phenylpropanoid and flavonoid pathways indicates activation of the entire anthocyanin biosynthetic program in purple-fleshed CIRAD136 rather than isolated regulation of individual enzymes.

The candidate set also contained known pigmentation transcriptional regulators [20,40–43]. Two *MYB* genes (*Dioal.02G036800.1* and *Dioal.13G060800.1*), three *WD40* (*Dioal.06G028100.1*, *Dioal.06G027900.1* and *Dioal.06G027200.1*) genes were more highly expressed in white-fleshed CIRAD137 than in purple-fleshed CIRAD136, while one *AP2* (*Dioal.03G021100.1*) gene showed up-regulation in CIRAD136. The coordinated expression of *AP2* with multiple structural genes across the anthocyanin pathway suggests that *Dioal.03G021100.1* represents a strong candidate regulator associated with activation of the anthocyanin biosynthetic program. However, whether *MYB* and WD40 candidates may participate in an alternative regulatory program associated with reduced anthocyanin accumulation requires functional validation [40,43–48].

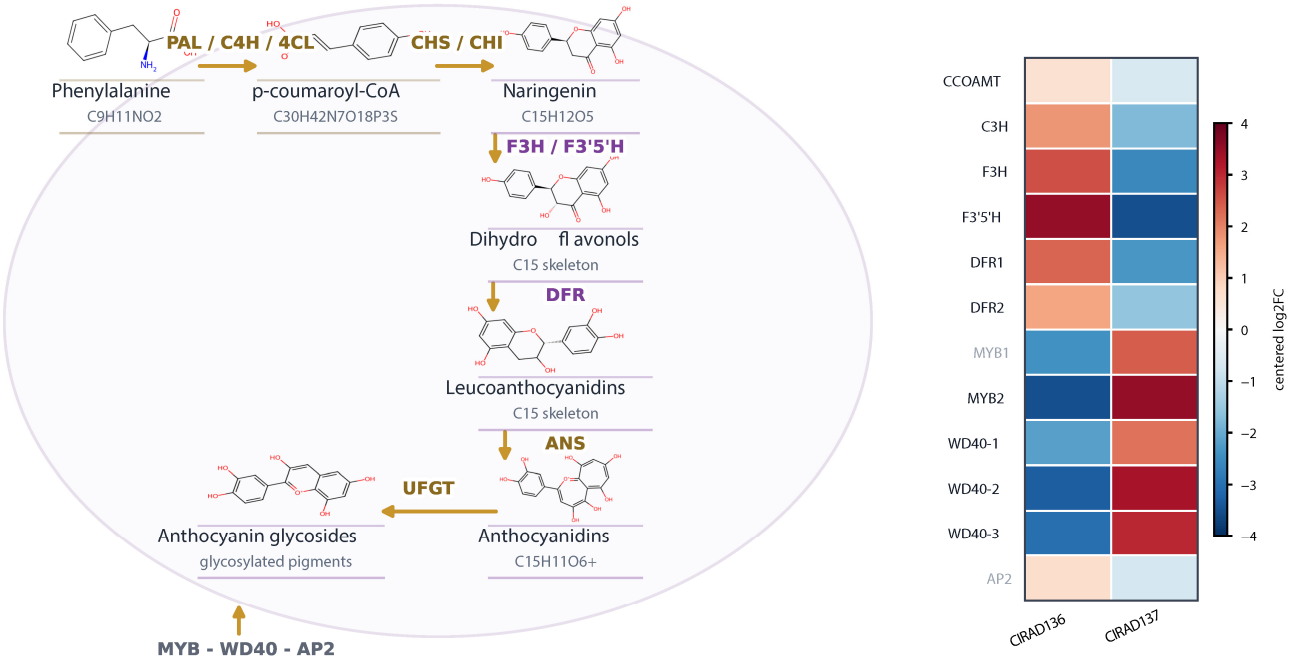


Figure 5. Anthocyanin candidate genes associated with purple tuber flesh. The figure summarizes a simplified phenylpropanoid-to-anthocyanin branch and a centered $\log_2$ fold-change heatmap for candidate structural and regulatory genes contrasting purple-fleshed variety CIRAD136 and white-fleshed variety CIRAD137. Key structural candidate genes identified in this study are: coumaroylquinate (coumaroyl shikimate) 3′-monooxygenase (*C3′H*), caffeoyl-CoA O-methyltransferase (*CCoAOMT*), flavonoid 3′-monooxygenase (*F3′H*), flavonoid 3′,5′-hydroxylase (*F3′5′H*) and bifunctional dihydroflavonol 4-reductase/flavanone 4-reductase (*DFR*). Gene names shown in black were also identified in other pairwise comparisons.

Carotenoid-related candidates were also identified. *Dioal.07G043100.1* (phytoene synthase; *PSY*) was more highly expressed in the yellow-fleshed CIRAD121 than in the white-fleshed CIRAD174 (Figure 6). As *PSY* catalyzes the first committed step of carotenoid biosynthesis, its up-regulation in CIRAD121 is consistent with a potential increase in carotenoid biosynthetic capacity [21,49]. Conversely, *Dioal.04G146000.1*, encoding 9-cis-epoxycarotenoid dioxygenase (*NCED*), was strongly up-regulated in the white-fleshed CIRAD174. Because *NCED* catalyzes carotenoid cleavage during abscisic acid biosynthesis [50,51], its elevated expression in CIRAD174 may be associated with enhanced carotenoid turnover and could contribute to lower carotenoid accumulation in this variety. Together, these expression patterns identify *PSY* and *NCED* as candidate genes potentially involved in tuber flesh coloration through carotenoid metabolism. However, carotenoid concentrations were not measured in this study, and therefore the proposed relationship between gene expression and carotenoid accumulation remains hypothetical and requires validation through targeted metabolite profiling and functional analyses.

3.6. Carbohydrate and Cell-Wall Candidates Link Expression Modules to Texture and Moldability

The "red" module was positively associated with soluble sugar concentration but negatively associated with starch granule area and tuber hardness (Table 2), suggesting coordinated regulation of carbon allocation between soluble sugar accumulation and starch deposition. Within this module, *Dioal.03G098300.1*, annotated as β-glucosidase 17 (*BG17*), together with two glycosyl hydrolase (*GH*) genes (*Dioal.08G028000.1*, GH1 and *Dioal.10G059200.1*, *GH2*), were prioritized as candidate genes (Figure 7). The two glycosyl hydrolase genes were more highly expressed in CIRAD154, a variety characterized by high soluble sugar content, low starch content and small starch granules, consistent with

enhanced carbohydrate turnover and mobilization [21,52]. Interestingly, *BG17* displayed an expression profile opposite to that of the glycosyl hydrolase genes, being more highly expressed in the high-starch genotype CIRAD137. Although its precise role in yam remains unclear, β-glucosidases have previously been implicated in tuber carbohydrate metabolism in potato [53], where their activity was associated with starch accumulation dynamics. These contrasting observations suggest that *BG17* may fulfill a distinct or species-specific role in carbohydrate metabolism in *D. alata*. Notably, no major differential expression was detected for key enzymes of the canonical starch biosynthetic pathway, including sucrose synthase, phosphoglucomutase, ADP-glucose pyrophosphorylase, starch synthase and starch-branching enzymes (Figure 7).

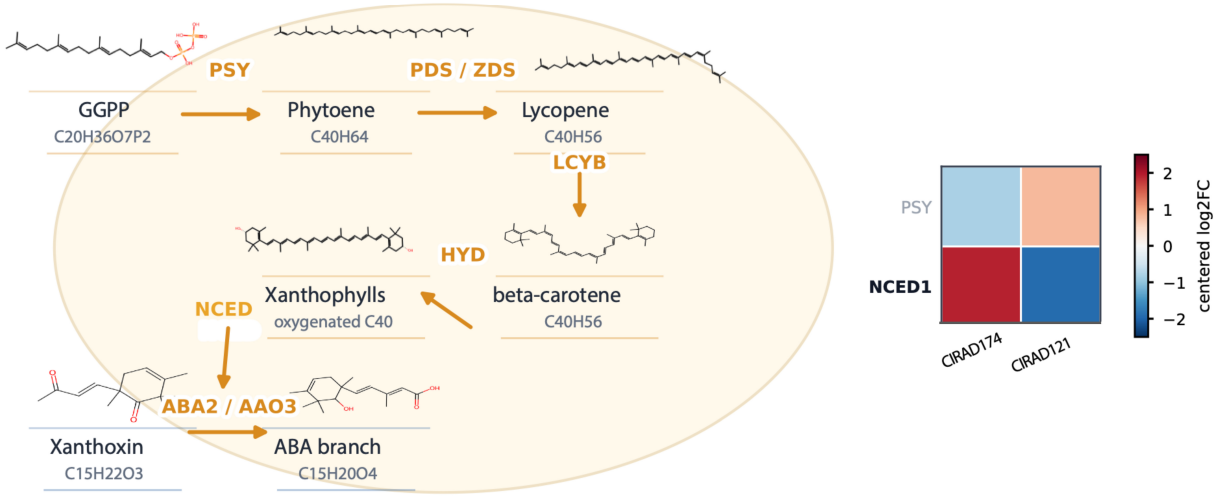


Figure 6. Carotenoid branch associated with yellow tuber flesh. The figure highlights the phytoene synthase (*PSY*) entry step, the 9-cis-epoxycarotenoid dioxygenase (*NCED*) carotenoid-cleavage branch and a centered $\log_2$ fold-change heatmap for candidates contrasting CIRAD121 and CIRAD174. Gene names shown in black were also identified in other pairwise comparisons.

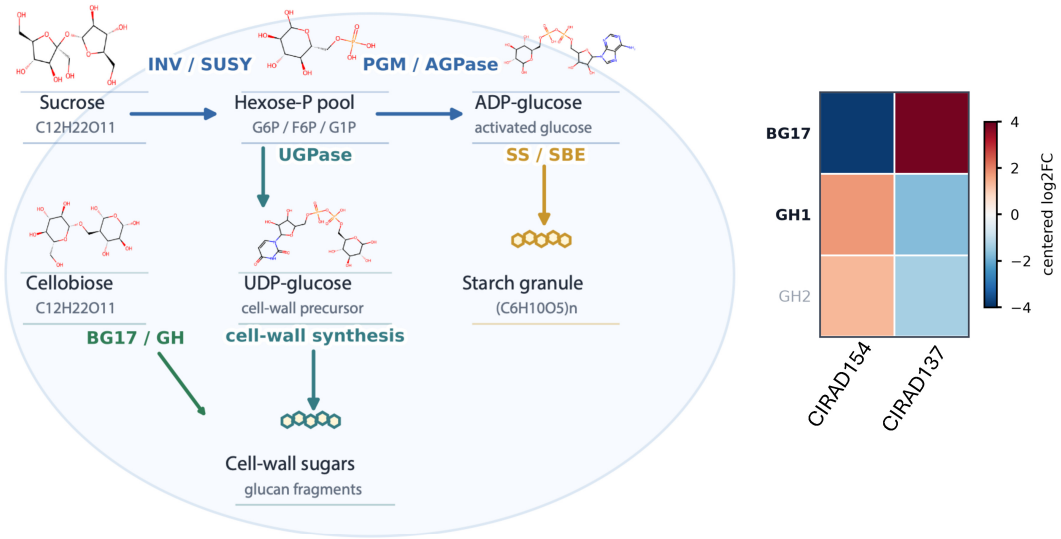


Figure 7. Carbohydrate turnover candidates linked to starch and sugar differences. The figure summarizes simplified sucrose/starch and cell-wall carbohydrate branches with a centered $\log_2$ fold-change heatmap for candidate beta-glucosidase and glycosyl hydrolase genes contrasting CIRAD137 and CIRAD154. Key structural candidate genes identified in this study are: beta glucosidase 17 (*BG17*) and glycoside hydrolase (*GH*). Gene names shown in black were also identified in other pairwise comparisons.

Candidate genes within the "orange" module included pectinesterases (*PMEs*), pectate lyases (*PLs*), galacturonidase (*GAL*) and aldo-keto reductases (*AKRs*), all involved in pectin metabolism and cell-wall modification (Figure 8). Rather than a uniform increase or decrease in all pectin-remodeling genes, contrasting expression patterns were observed among members of each gene family. For example, *PME2* and *PME4* were more highly expressed in the highly moldable variety CIRAD174, whereas *PME1* and *PME3* showed higher expression in the less moldable CIRAD121. Similar opposite expression patterns were observed among pectate lyase genes. These results suggest that moldability is governed by differential regulation of specific pectin-remodeling isoforms rather than by a generalized activation of pectin degradation. Collectively, the "orange" module supports a model in which coordinated remodeling of the pectin network modifies cell-wall architecture and intercellular adhesion, thereby influencing the mechanical properties and moldability of cooked yam tubers.

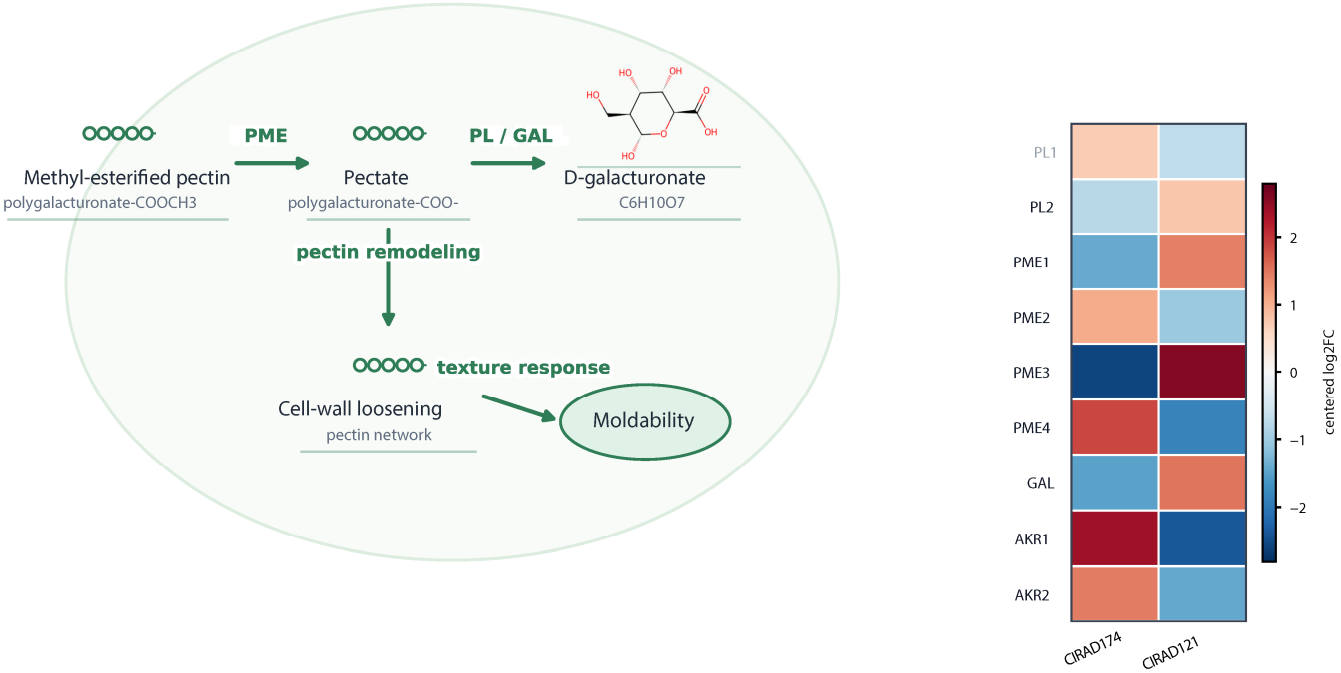


Figure 8. Pectin-remodeling candidates associated with moldability. The figure summarizes simplified pectin-remodeling steps and a centered $\log_2$ fold-change heatmap for pectinesterase (*PME*), pectate lyase (*PL*), galacturonidase (*GAL*) and Aldo-Keto Reductases (*AKR*) contrasting CIRAD174 and CIRAD121. Gene names shown in black were also identified in other pairwise comparisons.

3.7. qRT-PCR Analysis of the Expression Levels of Selected Candidate Genes

Fifteen candidate genes were selected for expression pattern analysis by qRT-PCR. These comprised six anthocyanin biosynthetic genes (*CCoAOMT*, *C3′H*, *F3′H*, *F3′5′H*, and two *DFR* genes), two carotenoid-related genes (*PSY* and one *NCED*), three putative pigmentation regulators, and four genes involved in carbohydrate metabolism and cell-wall modification, including a β-glucosidase, a glycosyl hydrolase/chitinase-like protein, a pectinesterase, and a galacturonidase. For normalization, *ACTIN18* was employed as the housekeeping gene, demonstrating robust stability across all six analyzed genotypes with a mean Ct of 21.83 ± 0.36 and a coefficient of variation of 1.35%. Based on this reliable baseline, qRT-PCR analyses of contrasting genotypes confirmed the RNA-seq expression patterns (Pearson correlation r = 0.962) for all selected genes (Figure 9; Supplementary Figure S2), thereby confirming their differential expression.

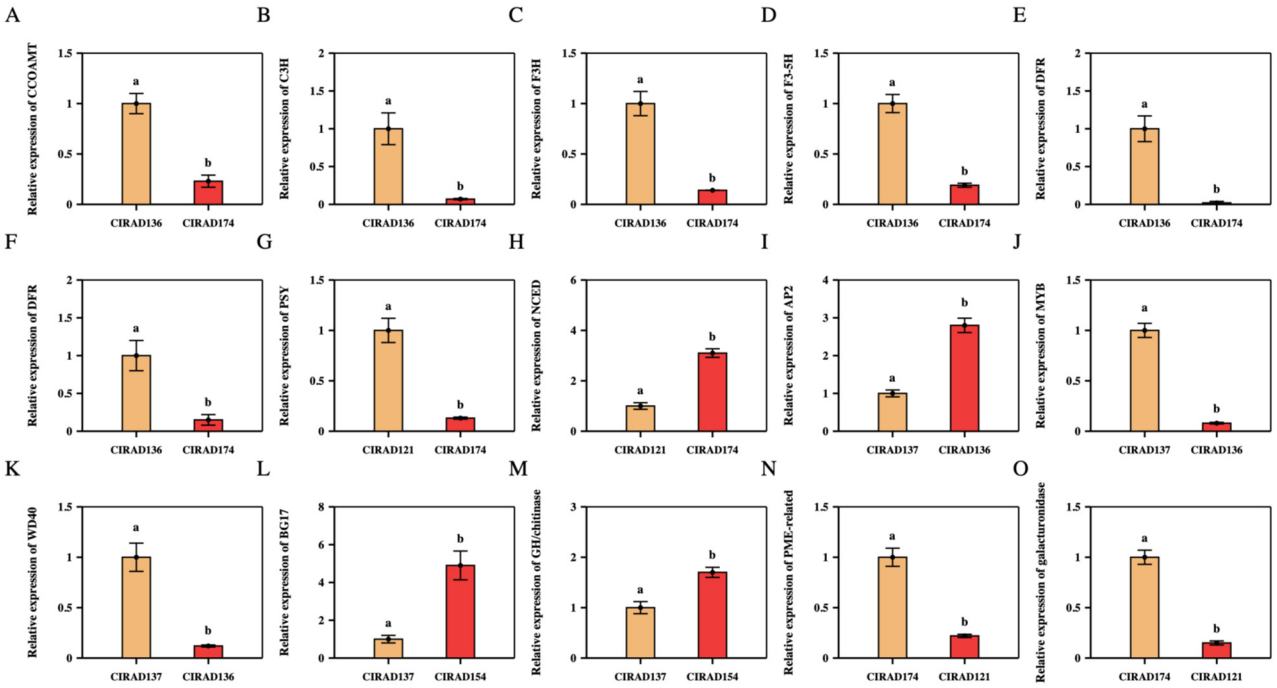


Figure 9. qRT-PCR validation of the expression patterns of 15 candidate genes associated with tuber flesh pigmentation, carotenoid/ABA metabolism, cell wall remodeling, and carbohydrate-related processes in contrasting *Dioscorea alata* genotypes. Bars represent the mean relative expression values normalized to the reference genotype for each comparison; error bars indicate standard deviations. Different letters above the bars indicate significant differences between genotypes according to Tukey's test. (**A**) *CCoAOMT* expression in CIRAD136 vs. CIRAD174; (**B**) *C3H* expression in CIRAD136 vs. CIRAD174; (**C**) *F3′H* expression in CIRAD136 vs. CIRAD174; (**D**) *F3′5′H* expression in CIRAD136 vs. CIRAD174; (**E**) *DFR* expression in CIRAD136 vs. CIRAD174; (**F**) *ANR* expression in CIRAD136 vs. CIRAD174; (**G**) *PSY* expression in CIRAD121 vs. CIRAD174; (**H**) *NCED* expression in CIRAD121 vs. CIRAD174; (**I**) *AP2* expression in CIRAD137 vs. CIRAD136; (**J**) *MYB* expression in CIRAD137 vs. CIRAD136; (**K**) *WD40* expression in CIRAD137 vs. CIRAD136; (**L**) *BG17* expression in CIRAD137 vs. CIRAD154; (**M**) GH/chitinase expression in CIRAD137 vs. CIRAD154; (N) PME-related expression in CIRAD174 vs. CIRAD121; (**O**) Galacturonidase expression in CIRAD174 vs. CIRAD121.

4. Discussion

A Co-Expression Network Framework Reveals the Molecular Architecture of Tuber Quality

This study provides a systems-level analysis of the molecular basis of tuber quality in greater yam. Previous transcriptomic studies in *D. alata* have primarily relied on pairwise comparisons [14–16]. Building upon these studies, the main contribution of this study lies beyond the identification of differentially expressed genes. By integrating transcriptomes from six phenotypically contrasting varieties with weighted gene co-expression network analysis, we identified co-expression modules associated with both varietal identity and contrasting tuber quality profiles. This network-based perspective extends previous studies from cataloguing individual DEGs to identifying biologically coherent regulatory programs associated with complex quality traits. Together, our findings indicate that the diverse components of tuber quality arise from interconnected molecular processes rather than a single regulatory pathway.

4.1. Pigmentation Candidates Validate Known Pathways and Extend Them to a Multi-Trait Context

Previous transcriptomic and metabolomic studies in *D. alata* have primarily focused on the molecular basis of purple flesh pigmentation, consistently identifying flavonoid biosynthetic genes, including *CHS*, *F3′H*, *DFR*, *ANS/LDOX* and glycosyltransferases, together with

cyanidin-derived anthocyanins, as the principal determinants of purple colouration [14–16]. Consistent with these studies, our analysis recovered *C3′H*, *F3′H*, *F3′5′H* and *DFR* among the strongest candidates differentiating purple- and white-fleshed genotypes, providing independent biological support for the robustness of our transcriptomic approach.

Beyond confirming previously reported structural genes, our study provides new insight into their upstream regulatory network. Anthocyanin biosynthesis is generally controlled by the conserved MYB-bHLH-WD40 (MBW) transcriptional complex, in which MYB proteins determine target specificity while WD40 proteins stabilize the regulatory complex [40–48]. *AP2/ERF* transcription factors have also emerged as important developmental regulators capable of modulating anthocyanin accumulation through transcriptional and hormonal signalling pathways [42]. Interestingly, unlike *AP2*, which was upregulated in the purple-fleshed genotype together with multiple anthocyanin structural genes, the identified *MYB* and *WD40* candidates displayed higher expression in the white-fleshed genotype. Although the canonical MBW complex is generally associated with activation of anthocyanin biosynthesis, numerous *MYB* proteins function instead as transcriptional repressors by replacing activating *MYBs* within the MBW complex or by preventing the formation of an active regulatory complex [43–46]. For example, *AtMYBL2* was found to be a key repressor of anthocyanin biosynthesis in *Arabidopsis thaliana* [47]. Zhu et al. [48] later discovered a *MYB* gene (*CPC*) that also negatively regulates anthocyanin biosynthesis in *A. thaliana.* The expression pattern observed in this study therefore suggests that the identified *MYB* candidates may participate in an alternative regulatory program limiting anthocyanin accumulation, whereas *Dioal.03G021100.1* (*AP2*) represents the strongest candidate regulator associated with activation of the anthocyanin biosynthetic program. Functional characterization will be required to determine whether these *MYB* genes indeed act as repressors in yam.

In contrast, the molecular basis of yellow flesh pigmentation remains largely unexplored in *D. alata*. Previous GWAS identified genomic regions associated with tuber flesh colour but did not resolve the underlying causal genes [12]. Unlike the purple-versus-white comparison, no *MYB*, *WD40* or *AP2* TFs were identified among the principal candidates differentiating yellow- and white-fleshed genotypes. Instead, *PSY*, encoding the rate-limiting enzyme of carotenoid biosynthesis, and *NCED*, which catalyses carotenoid cleavage towards ABA biosynthesis, emerged as the major candidate genes [21,49–51]. These results suggest that yellow flesh colour in greater yam may be associated with modulation of carotenoid metabolic flux through the balance between biosynthesis and degradation. Interestingly, transcriptomic and proteomic analyses of yellowing in Chinese yam (*D. polystachya*) also highlighted activation of carotenoid biosynthesis as a major contributor to yellow pigment accumulation, supporting the biological plausibility of the candidates identified here, although the underlying process involves post-harvest yellowing rather than natural flesh-colour variation [54].

Collectively, these findings indicate that purple and yellow flesh pigmentation in *D. alata* are potentially regulated through partially distinct molecular mechanisms. While purple pigmentation appears to depend on hierarchical transcriptional regulation involving *AP2* and the anthocyanin pathway, yellow pigmentation seems to be more closely associated with differential expression of carotenoid metabolic genes. This distinction highlights the value of co-expression network analysis for disentangling trait-specific regulatory architectures associated with flesh-colour variation in yam.

4.2. Carbohydrate and Cell-Wall Networks Reveal Complementary Mechanisms Associated with Yam Cooking Quality

Previous QTL mapping and GWAS in *D. alata* have identified genomic regions associated with dry matter content, starch concentration, cooking quality, hardness and

moldability [4,8,10,11,13]. While these studies demonstrated the complex genetic architecture of yam culinary quality, the biological mechanisms underlying these loci have remained largely unresolved. By integrating transcriptomic profiling with co-expression network analysis, the present study identifies two complementary biological processes, carbon allocation and cell-wall remodeling that provide a framework for interpreting these complex quality traits.

Carbohydrate composition is widely recognized as one of the principal determinants of yam culinary quality. Dry matter content, starch concentration, soluble sugar content and starch physicochemical properties collectively influence the texture, firmness and processing quality of boiled and pounded yam and therefore constitute major selection criteria in breeding programs [55,56]. Despite their agronomic importance, however, little is known about the transcriptional mechanisms associated with natural variation in these traits in *D. alata*. Unexpectedly, variation in starch content and soluble sugar concentration was not associated with differential expression of the canonical starch biosynthetic pathway. Instead of enzymes such as sucrose synthase, ADP-glucose pyrophosphorylase, starch synthases or starch-branching enzymes, the strongest candidates belonged to glycosyl hydrolase families involved in carbohydrate turnover and remobilization. This observation suggests that natural variation in tuber composition among the studied genotypes may be governed primarily by differences in carbon partitioning between soluble sugars and storage reserves rather than by transcriptional regulation of starch biosynthesis itself. Similar concepts have emerged from studies in potato and other storage organs, where sink strength and carbohydrate flux are increasingly recognized as important determinants of reserve accumulation in addition to the core starch biosynthetic enzymes [57,58].

The contrasting expression profiles of *BG17* and the glycosyl hydrolases further support this interpretation. Glycosyl hydrolases generally promote the hydrolysis of complex carbohydrates, thereby increasing soluble sugar availability and facilitating carbohydrate remobilization [59]. Their higher expression in the high-sugar genotype is therefore consistent with enhanced carbon turnover. Conversely, *BG17* accumulated preferentially in the high-starch genotype, suggesting a function distinct from the other hydrolases. Although its precise role remains unknown in yam, β-glucosidases have been implicated in storage organ development and carbohydrate metabolism in potato and other plant species, where they appear to contribute to developmental regulation beyond simple carbohydrate degradation [60]. One possibility is that *BG17* indirectly influences starch accumulation by regulating sink strength or carbon allocation.

Beyond carbohydrate metabolism, the present study identifies cell-wall remodeling as a second major biological process contributing to yam culinary quality. Among the strongest candidates, pectinesterases, pectate lyases and galacturan 1,4-α-galacturonidases consistently point to pectin remodeling as a central determinant of cooked-tuber mechanical properties [61]. Pectinesterases catalyse the de-methylesterification of homogalacturonan, thereby increasing the susceptibility of pectin polymers to degradation by pectate lyases and polygalacturonidases [62,63]. Through their coordinated activities, these enzymes regulate cell adhesion, cell-wall integrity and tissue firmness in numerous plant organs [62,64].

The higher expression of several pectinesterase, pectate lyase and galacturonidase genes in the less moldable genotype CIRAD121 suggests enhanced pectin remodeling and progressive disassembly of the middle lamella. Such changes are expected to weaken intercellular adhesion during cooking, thereby reducing the ability of boiled tubers to form the cohesive and elastic paste required for high-quality pounded yam. Similar mechanisms have been extensively documented during fruit softening, where coordinated regulation of pectin-modifying enzymes governs tissue mechanical properties through progressive remodeling of the cell wall [65,66].

Together, these findings support an integrated model in which yam culinary quality emerges from the interaction between intracellular carbohydrate partitioning and extracellular cell-wall integrity. While carbon allocation determines starch accumulation and soluble sugar balance, pectin remodeling governs tissue cohesion during cooking. The combination of these complementary biological processes is therefore likely to determine the mechanical behaviour of boiled tubers and their suitability for pounding. Future studies integrating transcriptomics with pectin chemistry, starch physicochemical characterization, tissue-mechanics measurements and functional validation will be required to establish the causal relationships underlying these candidate genes and ultimately facilitate their integration into molecular breeding strategies.

4.3. An Integrated View of Tuber Quality Provides Opportunities for Molecular Breeding

The co-expression modules identified in this study link biochemical composition with tuber morphology, including length-to-width ratio, skin texture and tubercular-root development. Although transcriptomic data obtained from mature tubers cannot establish causal relationships with developmental processes, these associations suggest that external morphology and internal quality are coordinated components of variety-specific developmental programs. Such integrated phenotypic profiles are particularly relevant because consumers and processors evaluate yam varieties based on the combined perception of appearance, texture and culinary performance rather than on individual biochemical traits [6,67].

From a breeding perspective, the integration of transcriptomic networks with phenotypic variation provides a biologically informed framework for prioritizing candidate genes for downstream validation. Our transcriptomic network approach can complement QTL and GWAS analyses by providing biologically plausible candidates within associated genomic regions. The increasing availability of chromosome-scale and haplotype-resolved yam genome assemblies [3,68,69] will further facilitate the integration of transcriptomic, structural variation and quantitative genetic data, accelerating marker development for quality-related traits.

A limitation of the present study is that RNA-seq was performed only at the mature tuber stage. Consequently, the observed expression differences may represent downstream metabolic consequences rather than the primary regulatory events associated with tuber development. Future studies should therefore adopt developmental time-course transcriptomics, ideally combined with metabolomics, pectin chemistry, starch physicochemical analyses and tissue-mechanics measurements, to reconstruct the temporal regulatory networks governing tuber quality. In addition, the application of long-read direct RNA sequencing represents a promising complementary approach to resolve full-length transcript isoforms, alternative splicing events and transcript processing, thereby providing a more comprehensive view of the regulatory mechanisms underlying complex tuber-quality traits [70]. A further limitation is the relatively small number of transcriptomes available for co-expression network analysis. Although the dataset showed satisfactory WGCNA diagnostic properties, the network was inferred from a limited number of samples. Larger independent datasets will be required to formally assess module preservation and refine these co-expression relationships.

Ultimately, functional validation will be essential to establish causal relationships between candidate genes and phenotype. Stable overexpression or CRISPR/Cas9-mediated genome editing of prioritized genes, together with gene-silencing approaches where appropriate, would enable direct assessment of their roles in pigmentation, carbohydrate metabolism and moldability. Recent advances in yam genetic transformation and genome editing provide promising opportunities to implement these strategies in *D. alata* and accelerate the translation of genomic discoveries into molecular breeding tools [71,72].

5. Conclusions

By integrating transcriptome profiling of multiple contrasting varieties with WGCNA, pathway annotation and targeted pairwise comparisons, this study identified coordinated co-expression modules associated with contrasting tuber quality profiles in *D. alata*. This systems-level approach enabled the prioritization of biologically meaningful candidate genes involved in pigmentation, carbohydrate metabolism and cell-wall remodeling, providing insights that could not be achieved through pairwise transcriptomic comparisons alone. The resulting regulatory framework constitutes a valuable resource for future genetic validation, functional genomics and molecular breeding aimed at improving yam culinary quality.

Supplementary Materials: The following supporting information can be downloaded at: https://www.mdpi.com/article/10.3390/horticulturae12101230/s1. Supplementary Table S1. qRT-PCR primers of 15 selected genes and *ACTIN18* in *Dioscorea alata;* Supplementary Table S2. RNA-seq quality-control and transcript quantification statistics for the 18 libraries representing six *Dioscorea alata* varieties; Supplementary Table S3. Differentially expressed genes across 15 pairwise variety comparisons. Only rows with padj < 0.05 were used in subsequent analyses; Supplementary Table S4. Top Kyoto Encyclopedia of gene and genomes pathway enrichment analysis with differentially expressed genes detected in this study; Supplementary Table S5. Stability statistics for all non-grey WGCNA modules across 18 leave-one-sample-out iterations; Supplementary Figure S1. Selection of the soft-thresholding power for WGCNA network construction; Supplementary Figure S2. Pearson correlation between $\log_2$FC qRT-PCR and $\log_2$FC RNA-seq expression data of 15 selected candidate genes across contrasting *D. alata* genotypes.

Author Contributions: Conceptualization, Q.Z., Y.L., K.D. and B.Y.; methodology, Q.Z., K.D. and E.M.; formal analysis, Q.Z., K.D. and Y.L.; investigation, E.M. and K.D.; visualization, Q.Z.; resources, Y.L. and B.Y.; writing—original draft preparation, Q.Z. and K.D.; writing—review and editing, Y.L., K.D. and B.Y.; supervision, Y.L., K.D. and B.Y.; project administration, K.D.; funding acquisition, Y.L., K.D. and B.Y. All authors have read and agreed to the published version of the manuscript.

Funding: This work was supported by the Jiangxi Provincial Health Commission Science and Technology Plan Project (No. 202311148), the Jiangxi Provincial Graduate Student Innovation Special Fund Project (No. YC2022-B025), the fund from the CGIAR Research Program on Roots, Tubers and Bananas (CRP-RTB) and European Union and Guadeloupe Region (Programme Opérationnel FEDER—Guadeloupe—Conseil Régional 2021–2027) project: TAESA (number: GPE005599).

Data Availability Statement: Transcriptome raw reads are available in the NCBI Sequence Read Archive, under the BioProject number: PRJNA918625 (https://www.ncbi.nlm.nih.gov/bioproject/?term=PRJNA918625, accessed on 10 May 2026).

Acknowledgments: We thank the BRC-TP for providing some yam accessions used in the present study. We used DeepL Write (https://www.deepl.com/write; accessed 14 July 2026) for English language editing. All suggestions were reviewed by the authors, who take full responsibility for the manuscript.

Conflicts of Interest: The authors declare no competing interests.

References

1. Asiedu, R.; Sartie, A. Crops that feed the world 1. *Yams. Food Secur.* **2010**, *2*, 305–315. [CrossRef]
2. Obidiegwu, J.E.; Lyons, J.B.; Chilaka, C.A. The *Dioscorea* genus (yam): An appraisal of nutritional and therapeutic potentials. *Foods* **2020**, *9*, 1304. [CrossRef]
3. Bredeson, J.V.; Lyons, J.B.; Oniyinde, I.O.; Okereke, N.R.; Kolade, O.; Nnabue, I.; Nwadili, C.O.; Hřibová, E.; Parker, M.; Nwogha, J.; et al. Chromosome evolution and the genetic basis of agronomically important traits in greater yam. *Nat. Commun.* **2022**, *13*, 2001. [CrossRef]

4. Zotta Mota, A.P.; Dossa, K.; Lechaudel, M.; Cornet, D.; Mournet, P.; Santoni, S.; Lopez, D.; Chair, H. Whole-genome sequencing and comparative genomics reveal candidate genes associated with quality traits in *Dioscorea alata*. *BMC Genom.* **2024**, *25*, 248. [CrossRef]
5. Barlagne, C.; Cornet, D.; Blazy, J.-M.; Diman, J.-L.; Ozier-Lafontaine, H. Consumers' preferences for fresh yam: A focus group study. *Food Sci. Nutr.* **2017**, *5*, 54–66. [CrossRef]
6. Honfozo, L.; Adinsi, L.; Bouniol, A.; Adetonah, S.; Forsythe, L.; Kleih, U.; Hounhouigan, J.D.; Fliedel, G.; Akissoe, N.H. Boiled yam end-user preferences and implications for trait evaluation. *Int. J. Food Sci. Technol.* **2021**, *56*, 1447–1457. [CrossRef]
7. Cormier, F.; Lawac, F.; Maledon, E.; Gravillon, M.-C.; Nudol, E.; Mournet, P.; Vignes, H.; Chaïr, H.; Arnau, G. A reference high-density genetic map of greater yam (*Dioscorea alata* L.). *Theor. Appl. Genet.* **2019**, *132*, 1733–1744. [CrossRef]
8. Gatarira, C.; Agre, P.; Matsumoto, R.; Edemodu, A.; Adetimirin, V.; Bhattacharjee, R.; Asiedu, R.; Asfaw, A. Genome-wide association analysis for tuber dry matter and oxidative browning in water yam (*Dioscorea alata* L.). *Plants* **2020**, *9*, 969. [CrossRef]
9. Ehounou, A.E.; Cornet, D.; Desfontaines, L.; Marie-Magdeleine, C.; Maledon, E.; Nudol, E.; Beurier, G.; Rouan, L.; Brat, P.; Lechaudel, M.; et al. Predicting quality, texture and chemical content of yam (*Dioscorea alata* L.) tubers using near infrared spectroscopy. *J. Near Infrared Spectrosc.* **2021**, *29*, 128–139. [CrossRef]
10. Ehounou, A.E.; Cormier, F.; Maledon, E.; Nudol, E.; Vignes, H.; Gravillon, M.-C.; N'guetta, A.S.P.; Chair, H.; Kouakou, A.M.; Gemma, A. Identification and validation of QTLs for tuber quality related traits in greater yam (*Dioscorea alata* L.). *Sci. Rep.* **2022**, *12*, 8423. [CrossRef]
11. Arnau, G.; Desfontaines, L.; Ehounou, A.E.; Marie-Magdeleine, C.; Kouakou, A.M.; Leinster, J.; Nudol, E.; Maledon, E.; Chair, H. Quantitative trait loci and candidate genes for physico-chemical traits related to tuber quality in greater yam (*Dioscorea alata* L.). *J. Sci. Food Agric.* **2024**, *104*, 4872–4879. [CrossRef]
12. Dossa, K.; Morel, A.; Houngbo, M.E.; Mota, A.Z.; Malédon, E.; Irep, J.-L.; Diman, J.-L.; Mournet, P.; Causse, S.; Van, K.N.; et al. Genome-wide association studies reveal novel loci controlling tuber flesh color and oxidative browning in *Dioscorea alata*. *J. Sci. Food Agric.* **2024**, *104*, 4895–4906. [CrossRef]
13. Dossa, K.; Houngbo, M.E.; Lechaudel, M.; Maledon, E.; Zoclanclounon, Y.A.B.; Irep, J.-L.; Nazir, M.F.; Chair, H.; Cornet, D. Detecting the genetic variants associated with key culinary traits in *Dioscorea alata*. *LWT* **2024**, *202*, 116301. [CrossRef]
14. Wu, Z.-G.; Jiang, W.; Nitin, M.; Bao, X.-Q.; Chen, S.-L.; Tao, Z.-M. Transcriptome analysis reveals flavonoid biosynthesis regulation and simple sequence repeats in yam (*Dioscorea alata* L.) tubers. *BMC Genom.* **2015**, *16*, 346. [CrossRef]
15. Wang, Y.; Lu, R.-S.; Li, M.-H.; Lu, X.-Y.; Sun, X.-Q.; Zhang, Y.-M. Unraveling the molecular basis of color variation in *Dioscorea alata* tubers: Integrated transcriptome and metabolomics analysis. *Int. J. Mol. Sci.* **2024**, *25*, 2057. [CrossRef]
16. Sun, J.; Zhuo, X.; Chen, X.; Wei, J.; Lin, J.; Shang, H.; Shan, N.; Huang, Y.; Zhou, Q.; Li, Z. Metabolome and transcriptome reveal the regulatory mechanism of anthocyanin synthesis in tuber skin and flesh of *Dioscorea alata* L. *Plants* **2025**, *14*, 3454. [CrossRef]
17. Srivichai, S.; Hongsprabhas, P. Profiling anthocyanins in Thai purple yams (*Dioscorea alata* L.). *Int. J. Food Sci.* **2020**, *2020*, 1594291. [CrossRef]
18. Grotewold, E. The genetics and biochemistry of floral pigments. *Annu. Rev. Plant Biol.* **2006**, *57*, 761–780. [CrossRef]
19. Tanaka, Y.; Sasaki, N.; Ohmiya, A. Biosynthesis of plant pigments: Anthocyanins, betalains and carotenoids. *Plant J.* **2008**, *54*, 733–749. [CrossRef]
20. Koes, R.; Verweij, W.; Quattrocchio, F. Flavonoids: A colorful model for the regulation and evolution of biochemical pathways. *Trends Plant Sci.* **2005**, *10*, 236–242. [CrossRef]
21. Stanley, L.; Yuan, Y.-W. Transcriptional regulation of carotenoid biosynthesis in plants: So many regulators, so little consensus. *Front. Plant Sci.* **2019**, *10*, 1017. [CrossRef]
22. Cao, T.; Wang, S.; Ali, A.; Shan, N.; Sun, J.; Chen, X.; Wang, P.; Zhu, Q.; Xiao, Y.; Luo, S.; et al. Transcriptome and metabolome analysis reveals the potential mechanism of tuber dynamic development in yam (*Dioscorea polystachya* Turcz.). *LWT* **2023**, *182*, 114764. [CrossRef]
23. Stuart, J.M.; Segal, E.; Koller, D.; Kim, S.K. A gene-coexpression network for global discovery of conserved genetic modules. *Science* **2003**, *302*, 249–255. [CrossRef]
24. Aoki, K.; Ogata, Y.; Shibata, D. Approaches for extracting practical information from gene co-expression networks in plant biology. *Plant Cell Physiol.* **2007**, *48*, 381–390. [CrossRef]
25. Langfelder, P.; Horvath, S. WGCNA: An R package for weighted correlation network analysis. *BMC Bioinform.* **2008**, *9*, 559. [CrossRef]
26. Ding, T.; Zhang, R.; Zhang, H.; Zhou, Z.; Liu, C.; Wu, M.; Wang, H.; Dong, H.; Liu, J.; Yao, J.L.; et al. Identification of gene co-expression networks and key genes regulating flavonoid accumulation in apple (*Malus* × *domestica*) fruit skin. *Plant Sci.* **2021**, *304*, 110747. [CrossRef]
27. Li, B.; Zhu, L.; Yang, N.; Qu, S.; Cao, W.; Ma, W.; Wei, X.; Ma, B.; Ma, F.; Fu, A.; et al. Transcriptional landscape and dynamics involved in sugar and acid accumulation during apple fruit development. *Plant Physiol.* **2024**, *195*, 2772–2786. [CrossRef]

28. Dossa, K.; Mmadi, M.A.; Zhou, R.; Zhang, T.; Su, R.; Zhang, Y.; Wang, L.; You, J.; Zhang, X. Depicting the core transcriptome modulating multiple abiotic stress responses in sesame (*Sesamum indicum* L.). *Int. J. Mol. Sci.* **2019**, *20*, 3930. [CrossRef]
29. Li, T.; Fan, Y.; Qin, H.; Dai, G.; Li, G.; Li, Y.; Wang, J.; Yin, Y.; Chen, F.; Qin, X.; et al. Transcriptome and flavonoids metabolomic analysis identifies regulatory networks and hub genes in black and white fruits of *Lycium ruthenicum* Murray. *Front. Plant Sci.* **2020**, *11*, 1256. [CrossRef]
30. Houngbo, M.E.; Desfontaines, L.; Irep, J.L.; Dibi, K.E.B.; Couchy, M.; Otegbayo, B.O.; Cornet, D. Starch granule size and shape characterization of yam (*Dioscorea alata* L.) flour using automated image analysis. *J. Sci. Food Agric.* **2024**, *104*, 4680–4688. [CrossRef]
31. Andrews, S. FastQC: A Quality Control Tool for High Throughput Sequence Data. 2010. Available online: https://www.bioinformatics.babraham.ac.uk/projects/fastqc/ (accessed on 14 January 2026).
32. Bolger, A.M.; Lohse, M.; Usadel, B. Trimmomatic: A flexible trimmer for Illumina sequence data. *Bioinformatics* **2014**, *30*, 2114–2120. [CrossRef]
33. Bray, N.L.; Pimentel, H.; Melsted, P.; Pachter, L. Near-optimal probabilistic RNA-seq quantification. *Nat. Biotechnol.* **2016**, *34*, 525–527, Correction in *Nat. Biotechnol*. **2016**, *34*, 888. [CrossRef]
34. Anders, S.; Huber, W. Differential expression analysis for sequence count data. *Genome Biol.* **2010**, *11*, R106. [CrossRef]
35. Love, M.I.; Huber, W.; Anders, S. Moderated estimation of fold change and dispersion for RNA-seq data with DESeq2. *Genome Biol.* **2014**, *15*, 550. [CrossRef]
36. Benjamini, Y.; Hochberg, Y. Controlling the false discovery rate: A practical and powerful approach to multiple testing. *J. R. Stat. Soc. Ser. B* **1995**, *57*, 289–300. [CrossRef]
37. Xie, C.; Mao, X.; Huang, J.; Ding, Y.; Wu, J.; Dong, S.; Kong, L.; Gao, G.; Li, C.-Y.; Wei, L. KOBAS 2.0: A web server for annotation and identification of enriched pathways and diseases. *Nucleic Acids Res.* **2011**, *39*, W316–W322. [CrossRef]
38. Kanehisa, M.; Sato, Y.; Kawashima, M.; Furumichi, M.; Tanabe, M. KEGG as a reference resource for gene and protein annotation. *Nucleic Acids Res.* **2016**, *44*, D457–D462. [CrossRef]
39. Livak, K.J.; Schmittgen, T.D. Analysis of relative gene expression data using real-time quantitative PCR and the $2^{-\Delta\Delta CT}$ method. *Methods* **2001**, *25*, 402–408. [CrossRef]
40. Xu, W.; Dubos, C.; Lepiniec, L. Transcriptional control of flavonoid biosynthesis by MYB–bHLH–WDR complexes. *Trends Plant Sci.* **2015**, *20*, 176–185. [CrossRef]
41. Yan, H.; Pei, X.; Zhang, H.; Li, X.; Zhang, X.; Zhao, M.; Chiang, V.L.; Sederoff, R.; Zhao, X. MYB-mediated regulation of anthocyanin biosynthesis. *Int. J. Mol. Sci.* **2021**, *22*, 3103. [CrossRef]
42. Chen, L.; Cheng, Y.; Hong, G. Molecular insights into the regulation of flavonoid biosynthesis in fruits. *Hortic. Res.* **2026**, *13*, uhaf306. [CrossRef]
43. Albert, N.W.; Davies, K.M.; Lewis, D.H.; Zhang, H.; Montefiori, M.; Brendolise, C.; Boase, M.R.; Ngo, H.; Jameson, P.E.; Schwinn, K.E. A conserved network of transcriptional activators and repressors regulates anthocyanin pigmentation in eudicots. *Plant Cell* **2014**, *26*, 962–980. [CrossRef]
44. Ma, D.; Constabel, C.P. MYB repressors as regulators of phenylpropanoid metabolism in plants. *Trends Plant Sci.* **2019**, *24*, 275–289. [CrossRef]
45. Chen, L.; Hu, B.; Qin, Y.; Hu, G.; Zhao, J. Advance of the negative regulation of anthocyanin biosynthesis by MYB transcription factors. *Plant Physiol. Biochem.* **2019**, *136*, 178–187. [CrossRef]
46. LaFountain, A.M.; Yuan, Y.-W. Repressors of anthocyanin biosynthesis. *New Phytol.* **2021**, *231*, 933–949. [CrossRef]
47. Matsui, K.; Umemura, Y.; Ohme-Takagi, M. AtMYBL2, a protein with a single MYB domain, acts as a negative regulator of anthocyanin biosynthesis in Arabidopsis. *Plant J.* **2008**, *55*, 954–967. [CrossRef]
48. Zhu, H.-F.; Fitzsimmons, K.; Khandelwal, A.; Kranz, R.G. CPC, a single-repeat R3 MYB, is a negative regulator of anthocyanin biosynthesis in Arabidopsis. *Mol. Plant* **2009**, *2*, 790–802. [CrossRef]
49. Ruiz-Sola, M.A.; Rodríguez-Concepción, M. Carotenoid biosynthesis in Arabidopsis: A colorful pathway. *Arab. Book* **2012**, *10*, e0158. [CrossRef]
50. Tan, B.-C.; Joseph, L.M.; Deng, W.-T.; Liu, L.; Li, Q.-B.; Cline, K.; McCarty, D.R. Molecular characterization of the Arabidopsis 9-cis-epoxycarotenoid dioxygenase gene family. *Plant J.* **2003**, *35*, 44–56. [CrossRef]
51. Dhar, M.K.; Mishra, S.; Bhat, A.; Chib, S.; Kaul, S. Plant carotenoid cleavage oxygenases: Structure–function relationships and role in development and metabolism. *Brief. Funct. Genom.* **2020**, *19*, 1–9. [CrossRef]
52. van Harsselaar, J.K.; Lorenz, J.; Senning, M.; Sonnewald, U.; Sonnewald, S. Genome-wide analysis of starch metabolism genes in potato (*Solanum tuberosum* L.). *BMC Genom.* **2017**, *18*, 37. [CrossRef]
53. Yu, C.; Yu, X.; Jiang, B.; Liu, Z.; Li, H.; Ao, X.; Wang, J.; Qiu, P.; Zhang, L.; Bai, J.; et al. Uncovering key genes related to potato tuber starch concentration from the tuber bulking, maturation stage to storage. *bioRxiv* **2026**, 2026.07.28.741397. [CrossRef]
54. Guo, S.; Wang, D.; Ma, Y.; Zhang, Y.; Zhao, X. Combination of RNA-seq transcriptomics and iTRAQ proteomics reveal the mechanism involved in fresh-cut yam yellowing. *Sci. Rep.* **2021**, *11*, 7755. [CrossRef]

55. Akissoe, N.; Mestres, C.; Handschin, S.; Gibert, O.; Hounhouigan, J.; Nago, M. Microstructure and physico-chemical bases of textural quality of yam products. *LWT Food Sci. Technol.* **2011**, *44*, 321–329. [CrossRef]
56. Otegbayo, B.; Oroniran, O.; Tanimola, A.R.; Fawehinmi, B.; Alamu, A.; Bolaji, T.; Madu, T.; Okoye, B.; Chijioke, U.; Ofoeze, M.; et al. Food quality profile of pounded yam and implications for yam breeding. *J. Sci. Food Agric.* **2024**, *104*, 4635–4651. [CrossRef]
57. Geigenberger, P. Regulation of starch biosynthesis in response to a fluctuating environment. *Plant Physiol.* **2011**, *155*, 1566–1577. [CrossRef]
58. Tetlow, I.J.; Emes, M.J. A review of starch-branching enzymes and their role in amylopectin biosynthesis. *IUBMB Life* **2014**, *66*, 546–558. [CrossRef]
59. Minic, Z. Physiological roles of plant glycoside hydrolases. *Planta* **2008**, *227*, 723–740. [CrossRef]
60. Morant, A.V.; Jørgensen, K.; Jørgensen, C.; Paquette, S.M.; Sánchez-Pérez, R.; Møller, B.L.; Bak, S. β-Glucosidases as detonators of plant chemical defense. *Phytochemistry* **2008**, *69*, 1795–1813. [CrossRef]
61. Effah-Manu, L.; Maziya-Dixon, B.; Wireko-Manu, F.D.; Agbenorhevi, J.K.; Oduro, I. Yam pectin and textural characteristics: A preliminary study. *Int. J. Food Prop.* **2022**, *25*, 1591–1603. [CrossRef]
62. Wolf, S.; Mouille, G.; Pelloux, J. Homogalacturonan methyl-esterification and plant development. *Mol. Plant* **2009**, *2*, 851–860. [CrossRef]
63. Sénéchal, F.; Wattier, C.; Rustérucci, C.; Pelloux, J. Homogalacturonan-modifying enzymes: Structure, expression, and roles in plants. *J. Exp. Bot.* **2014**, *65*, 5125–5160. [CrossRef]
64. Wang, D.; Yeats, T.H.; Uluisik, S.; Rose, J.K.C.; Seymour, G.B. Fruit softening: Revisiting the role of pectin. *Trends Plant Sci.* **2018**, *23*, 302–310. [CrossRef]
65. Brummell, D.A. Cell wall disassembly in ripening fruit. *Funct. Plant Biol.* **2006**, *33*, 103–119. [CrossRef]
66. Majumdar, R.; Strausbaugh, C.A.; Galewski, P.J.; Minocha, R.; Rogers, C.W. Cell-wall-degrading enzymes-related genes originating from Rhizoctonia solani increase sugar beet root damage in the presence of *Leuconostoc mesenteroides*. *Int. J. Mol. Sci.* **2022**, *23*, 1366. [CrossRef]
67. Mazza, M.A.; Nnabue, I.; Oselebe, H.; Darkwa, K.; Konan, D.; Dansi, A.; Otoo, E.; Adebola, P.O.; Agre, P.; Wossen, T.; et al. Farmer trait preferences and implications for demand-led yam breeding in selected production areas of West Africa. *Front. Sustain. Food Syst.* **2026**, *10*, 1757206. [CrossRef]
68. Zhang, Y.-M.; Wei, Z.-Y.; Yang, C.-A.; Feng, X.-Y.; Wang, Y.; Li, S.-X.; Sun, X.-Q.; Shao, Z.-Q.; Xue, J.-Y. A telomere-to-telomere genome assembly for greater yam (*Dioscorea alata*). *Plant Commun.* **2025**, *6*, 101326. [CrossRef]
69. Dossa, K.; Su, X.; Zoclanclounon, Y.A.B.; Chen, Y.; Nawaz, M.A.; Ni, P.; Qiu, T.; Chen, G.; Malédon, E.; Gravillon, M.-C.; et al. Haplotype-resolved genome assembly of a male *Dioscorea alata* cultivar reveals the structure and evolution of young sex chromosomes. *Plant J.* **2026**, *127*, e71091. [CrossRef]
70. Zhang, T.; Li, J.; Tang, C.; Wu, Y.; Wu, H.; Zhu, X.-T.; Luo, Z.; Qin, H.; Ding, L.; Zeng, Y. Nanopore Direct RNA Sequencing and the Epitranscriptome: Advances in Mapping Native RNA Landscapes. *iMeta* **2026**, *5*, e70136. [CrossRef]
71. Nyaboga, E.; Tripathi, J.N.; Manoharan, R.; Tripathi, L. Agrobacterium-mediated genetic transformation of yam (*Dioscorea* rotundata): An important tool for functional study of genes and crop improvement. *Front. Plant Sci.* **2014**, *5*, 463. [CrossRef]
72. Syombua, E.D.; Zhang, Z.; Tripathi, J.N.; Ntui, V.O.; Kang, M.; George, O.O.; Edward, N.K.; Wang, K.; Yang, B.; Tripathi, L. A CRISPR/Cas9-based genome-editing system for yam (*Dioscorea* spp.). *Plant Biotechnol. J.* **2021**, *19*, 645–647. [CrossRef]

Disclaimer/Publisher's Note: The statements, opinions and data contained in all publications are solely those of the individual author(s) and contributor(s) and not of MDPI and/or the editor(s). MDPI and/or the editor(s) disclaim responsibility for any injury to people or property resulting from any ideas, methods, instructions or products referred to in the content.